submitted to *Geophys. J. Int.*

Locking depth and slip-rate of the Húsavík Flatey fault, North Iceland, derived from continuous GPS data 2006-2010

Sabrina Metzger[1] ⋆, Sigurjón Jónsson[2] and Halldór Geirsson[3,4]

[1] *Institute of Geophysics, ETH Zürich, Sonneggstrasse 5, 8092 Zürich, Switzerland*

[2] *King Abdullah University of Science and Technology (KAUST), Thuwal, Saudi Arabia*

[3] *The Pennsylvania State University, University Park, Pennsylvania, USA*

[4] *Icelandic Meteorological Office (IMO), Reykjavík, Iceland*

21 June 2011

SUMMARY

Located at the northern shore of Iceland, the Tjörnes Fracture Zone (TFZ) is a 120 km offset in the Mid-Atlantic Ridge that connects the offshore Kolbeinsey Ridge to the on-land Northern Volcanic Zone. This transform zone is seismically one of the most active areas in Iceland, exposing the population to a significant risk. However, the kinematics of the mostly offshore area with its complex tectonics have not been adequately resolved and the seismic potential of the two main transform structures within the TFZ, the Grímsey Oblique Rift, and the Húsavík Flatey fault in particular, is not well known.

In summer 2006, we expanded the number of continuous GPS (CGPS) stations in the area from 4 to 14. The resulting GPS velocities after 4 years of data collection show that the TFZ accommodates the full plate motion as it is predicted by the MORVEL plate motion model. In addition, ENVISAT interferograms reveal a transient uplift signal at the nearby Theistareykir central volcano with a maximum line-of-sight uplift of 3 cm between summers of 2007 and 2008. We use a combination of an interseismic back-slip and a Mogi model in a homogeneous, elastic half-space to describe the kinematics within the TFZ. With a non-linear optimization approach we fit the GPS observations and estimate the key model parameters and their uncertainties, which are (among others) the locking depth, the partition of the transform motion between the two transform structures within the TFZ and the slip rate on the Húsavík Flatey fault.

We find a shallow locking depth of $6.7^{+1.8}_{-1.3}$ km and transform motion that is accommodated 34±3% by the Húsavík Flatey fault and 66±3% by the Grímsey Oblique Rift, resulting in a slip velocity of 6.8±0.7 mm/yr for the Húsavík Flatey fault. Assuming steady accumulation since the last two large M6.5 earthquakes in 1872 the seismic potential of the fault is equivalent to a M_w6.8±0.1 event.

1 INTRODUCTION

The Tjörnes Fracture Zone (TFZ) in North Iceland is a ∼120 km offset in the Mid-Atlantic Ridge that at this latitude is spreading with a rate of 18 mm/yr (MORVEL, DeMets et al. 2010). During the past 140 years no major earthquake has released the stress that likely has accumulated on the transform Húsavík Flatey fault (HFF), one of the main structures within the TFZ. Húsavík is the second largest town in North Iceland (2,300 people, Fig. 1), located directly on top of the HFF and therefore exposed to a high seismic risk. In addition, discussions of significant industrial development for the Húsavík area have risen during the past decade, which would include the construction of an aluminum smelter (Hönnun engineering consultants 2005; Alcoa press release 2006). It is therefore both of interest and importance to shed light on the plate kinematics within the TFZ and to assess the potential seismic hazard of the HFF.

Key parameters for evaluating the seismic hazard are the slip velocity and the locking depths of the main locked fault segments within a seismogenic zone (e.g. Wesnousky 1986). A seismotectonic analysis of Rögnvaldsson et al. (1998) indicated a locking depth of 10-12 km in the Tjörnes Fracture Zone. Based on that assumption Jouanne et al. (2006) modeled campaign GPS data from 1997-2002 and found a 8 mm/yr velocity difference over a 25 km profile across the HFF in the Húsavík area. Geirsson et al. (2006) evaluated the velocities of three continuous GPS (CGPS) stations in North Iceland and estimated the motion on HFF to be 40% of the total transform motion across the TFZ. Assuming a MORVEL velocity of 18 mm/yr (DeMets et al. 2010) the slip rate on the HFF would be 7 mm/yr. Árnadóttir et al. (2009) modeled nationwide campaign GPS observations from 1993 and 2004 and found a slip rate of 5 mm/yr for the HFF and a relatively shallow but - due to the sparsity of stations in the TFZ - rather poorly constrained locking depth of $\sim$5 km.

In this paper we analyze the surface deformation in the TFZ and describe a kinematic model of the TFZ as a whole and of the HFF in particular, based primarily on CGPS data from 2006-2010. We also use InSAR data to analyze inflation at Theistareykir central volcano. We then estimate the optimal model parameters of locking depth and fault motion to assess the slip deficit that has accumulated on the Húsavík Flatey fault plane since the last two big earthquakes in 1872 and hence the seismic potential of the fault.

2 TECTONIC SETTING AND EARTHQUAKE ACTIVITY

Iceland is located on the Mid-Atlantic Ridge (MAR) with the West being part of the North American plate and the East belonging to the Eurasian plate. The plate boundary zone is a few tens of kilometers wide and is characterized by a set of transforms and volcanic zones (Einarsson 2008, and Fig. 1). The transform zones are located in the coastal areas and connect the offshore sections of the MAR with the onshore volcanic zones. In the South, the South Icelandic Seismic Zone connects the Eastern Volcanic Zone to the Reykjanes Peninsula Oblique Rift, which is a continuation of the Reykjanes Ridge southwest of Iceland. In the North the Tjörnes Fracture Zone (TFZ) links the Kolbeinsey Ridge to the Northern Volcanic Zone (NVZ). Both transform zones accommodate mainly trans-current motion, are seismically highly active and produce the largest earthquakes in Iceland (Tryggvason 1973; Stefánsson 1979; Einarsson 2008).

Plate spreading across North Iceland is occurring at a rate of 18 mm/yr with an azimuth of N105°E (MORVEL plate motion model, DeMets et al. 2010). Árnadóttir et al. (2009) used CGPS data from 1999-2004 and nationwide GPS campaign data from 1993 and 2004 to derive a kinematic model of the plate spreading across Iceland with several dislocations representing the different segments of the plate boundary. They found a slightly elevated spreading rate in the Northern Volcanic Zone of 23$\pm$2 mm/yr and suggested that this elevated rate was due to post-rifting relaxation after the 1975-1984 Krafla rifting episode (e.g. Björnsson 1985; Einarsson 1991). The first

GPS campaigns around the Krafla fissure swarm (1987-1992) were carried out to study this post-rifting transient and they showed a pulse of extension across the area that decayed in amplitude with time and propagated away from the rift axis (Foulger et al. 1992; Heki et al. 1993; Hofton & Foulger 1996). The following GPS campaigns further showed the decaying pulse approaching the long-term average extension rates (Völksen 2000).

Earthquakes occur mainly along two main seismic lineaments in the TFZ, the HFF and the Grímsey Oblique Rift (GOR, Fig. 1). A M6.2 in 1934 close to the town of Dalvík and an offshore M7 earthquake $\sim$60 km northwest of Dalvík in 1963 suggest a third parallel lineament to the Southwest of the HFF (Einarsson 1991; Stefánsson et al. 2008). However, no surface expression of this seismic lineament has been identified (Rögnvaldsson et al. 1998; Långbacka & Gudmundsson 1995). A seismotectonic analysis of micro-earthquake clusters provided more insight into the TFZ (Rögnvaldsson et al. 1998): The offshore GOR consists of a set of *en echelon* faults with steeply dipping (70°-90°) planes. They are mostly N-S-oriented and align from Grímsey towards Öxarfjörður. This geometry is sometimes called *bookshelf faulting* and has also been proposed in the South Icelandic Seismic Zone and the Reykjanes Peninsula (Einarsson 1991). McMaster et al. (1977) carried out bathymetry, magnetics and seismic reflection measurements offshore North Iceland and reported a series of graben-like troughs with a N-S trend. Also, the GOR is volcanically active (Brandsdóttir et al. 2005). These studies indicate that both normal and strike-slip faulting takes place in the area, similar to the Reykjanes Ridge.

In contrast, the HFF is a system of WNW-oriented right-lateral strike-slip faults with no apparent volcanism. Its strands origin at the Theistareykir fissure swarm in the East as a NW-oriented fault and enters the sea at Húsavík. West of Húsavík, the offshore part of the HFF has a slightly more WNW-orientation (Fig. 1) and can be continuously traced in bathymetric data (Brandsdóttir et al. 2005). The HFF passes between the Flateyarskagi peninsula and the Flatey island and connects finally to the Eyjarfjarðaráll Rift that extends to the Kolbeinsey Ridge. The fault bend at Húsavík adds an opening component to the fault segment southeast of the town. This entails the generation of the two sag ponds (pull-apart basins) aligning with the surface fault traces close to Húsavík (see mapped fault traces in Figure 1). The western part of the HFF is well-defined by seismicity, but the eastern part shows a lack of seismicity (Einarsson 1991), apparently due to the Krafla rifting episode (see below).

Estimated locations and magnitudes of historical earthquakes in North Iceland, based on reported damage, are not accurate and have to be treated with a notable uncertainty. The most important earthquakes of the last 300 years within the TFZ are shown in Figure 1 (after Stefánsson et al. 2008). In 1885 a M6.3 struck a southeastern part of the GOR and a M7 earthquake occurred along its central part in 1910. The last significant earthquake was of M6.2, located in the Öxarfjörður bay, where the Krafla fissure swarm connects to the GOR. This event happened in 1976 during the initial phase of the Krafla rifting episode (e.g. Tryggvason 1980; Björnsson 1985; Einarsson 1991). Four major earthquakes occurred on the HFF during the past 200 years. In 1755, an earthquake with an estimated M7 took place in Skjálfandi bay and a M6.5 occurred near its western end in 1838. The last major earthquake sequence on the eastern part of the HFF occurred 1872 with the two largest events reaching M6.5, located close to Flatey and Húsavík. Most of the present-day seismicity of HFF is located on the northwestern part of the fault (Fig. 1). Due to their offshore location the earthquake depths are not well constrained by the present seismic network geometry. Rögnvaldsson et al. (1998) reanalyzed 60 earthquake swarms of 1994-1998 in the TFZ, mostly on the HFF and the GOR, and after relocating 1400 earthquakes they found that more than 90% of the events in the TFZ occur at depths shallower than 10 km.

The eastern end of the HFF links to the Theistareykir volcanic system, which is part of the NVZ. Ash layer dating revealed that the glacial retreat at the end of the last ice age set in relatively early and was followed by a pulse of volcanic activity in the area, causing an eruption $\sim$ 12,000 yr BP on Theistareykjarbunga, a shield volcano slightly Northeast of what is nowadays believed to be the central volcano (see Fig. 1, Karl Grönvold, pers. comm. 2011). After a long period of inactivity, another eruption right at the Theistareykir central volcano took place $\sim$ 9,000 yr BP. The last and most recent eruption happened $\sim$ 2,500 yr BP, forming the lava flow "Theistareykjahraun" between the central volcano and the HFF. This intact lava field is also evidence for absence of any rifting in the area since its formation (Karl Grönvold, pers. comm. 2011). In the next volcanic system southeast of Theistareykir, Krafla, large extensions of several meters in

E-W direction occurred during the 1975-1984 rifting episode. The extension was accompanied by a couple of M5-6.5 earthquakes (e.g. Tryggvason 1980; Björnsson 1985; Tryggvason 1984). The average horizontal displacement across the Krafla fissure swarm was 5 m, which corresponds to 275 years of opening in North Iceland (assuming 18.1 mm/yr). After that rifting episode the microseismicity on the southeastern end of HFF decreased significantly (Rögnvaldsson et al. 1998) and has not yet recovered (Fig. 1).

3 PREVIOUS GPS MEASUREMENTS AND MODELING RESULTS IN NORTH ICELAND

The first two continuous GPS stations in Iceland were installed in Reykjavík (REYK, 1995) in the Southwest and Höfn (HOFN, 1997) in the Southeast (Fig. 1). They are part of the International GNSS Service (IGS) reference network. In 1999, a cooperative project between the Icelandic Meteorological Office (IMO) and several other institutions initiated a continuous GPS network of approximately 20 stations with a particular focus on active geophysical processes along the plate boundary (Geirsson et al. 2006). The first stations in North Iceland started operation in summer of 2001. The National Land Survey of Iceland set up a station in Akureyri (AKUR, on the North American plate) and the Université de Savoie, France, together with IMO, installed the station RHOF in Raufarhöfn, located on the Eurasian plate, and one year later, in summer 2002, the station ARHO on the Tjörnes peninsula midway between AKUR and RHOF (Fig. 1). In 2006/2007, the CGPS network in Iceland was again expanded by the cooperation of IMO and four universities (University of Iceland, University of Arizona, The Pennsylvania State University, ETH Zürich). The purpose is to study steady state and transient deformation due to plate spreading, volcanic activity, earthquakes and uplift due to glacio-isostatic adjustments (Árnadóttir et al. 2008). After this expansion a total of 64 continuous GPS stations were operating in Iceland by early 2010 (Geirsson et al. 2010) and 14 of them are located in North Iceland.

Before the CGPS network was installed, numerous GPS campaigns provided surface deformation data in North Iceland. Hofton & Foulger (1996) performed GPS campaigns in North Iceland from 1986 to 1992 to study the post-rifting of Krafla. Árnadóttir et al. (2009) modeled the Icelandic plate spreading and glacial uplift with countrywide GPS campaign data (ISNET) of 1993 and 2004, as mentioned above. Their model included discrete discontinuities for the HFF and the GOR. Due to the sparse network and the offshore location of the TFZ the plate boundary model produced rather poorly resolved parameters for both structures. The locking depth for the GOR was estimated with 4-15 km with a slip rate of 9-22 mm/yr and for the HFF the locking depth $\sim$5 km with a slip rate of $<$5 mm/yr. This low rate does not agree with the slip rate estimation based on the data from the three continuous stations AKUR, ARHO and RHOF that was published by Geirsson et al. (2006). They found that the total spreading motion of North Iceland was partitioned between the HFF and GOR with a ratio of 40/60 percent, which results in a slip velocity of $\sim$7 mm/yr, given the MORVEL velocity of 18 mm/yr (DeMets et al. 2010).

A network of 50 campaign GPS markers in the TFZ that spans a 100 km by 80 km area has been measured seven times from 1995 to 2010 to study the ongoing deformation in the region (Jouanne et al. 1999, 2006). Between the two time spans 1997-1999 and 1999-2002 a decrease of the overall spreading rate was observed and explained with post-rifting relaxation of the Krafla rifting episode (Jouanne et al. 2006). Velocities of GPS stations near the central portion of the HFF, on Flatey island and Flateyjarskagi, differed only within uncertainties and did not provide information about the lockage of the fault. In contrast, station velocities along a 25-km-long profile across the HFF at Húsavík show a change of 8 mm/yr so the authors suggested the locking depth to be larger than 10-12 km.

4 GPS DATA

4.1 CGPS Network Installation

To gain further insight into the strain accumulation on the HFF and the tectonics of the TFZ, we complemented the North Iceland continuous GPS network (AKUR/ARHO/RHOF/MYVA) with additional ten GPS receivers to a total of 14 stations (Fig. 1). The network covers an area of 150 km by 100 km and is centered around the town of Húsavík. The wide-range surface deformation of the TFZ is observed by eight stations, which includes receivers on the islands Flatey (FTEY) and Grímsey (GMEY). In addition, a profile of six CGPS stations crosses the HFF near Húsavík and records the deformation near the fault. The station MYVA south of the TFZ is locally affected by local deformation processes of the Krafla volcanic system and thus could not be used for this study. On the other hand, HEID, a semi-permanent station in East Iceland (see inset in Fig. 1), was included into the estimation of the deformation model parameters because of its defintive location inside the Eurasian plate. A station overview including coordinates and information on GPS receiver and antenna types is given in Table 1.

An inherent problem of investigating the deformation across the TFZ is its mostly submarine location, where conventional geodetic techniques to measure crustal deformation do not apply. An effort was made to place the GPS stations strategically to constrain the kinematics of the TFZ as well as possible. In addition there was generally a trade-off between surface conditions and site accessibility in terms of access roads, power and data transmission. All stations were put on solid rock that endured glacial erosion except station GAKE that was installed on a post-glacial lava flow and station FTEY on Flatey island, whose foundations were drilled into consolidated sediments. We installed the stations close to farms or houses for electricity whenever possible and most of the stations make use of the existing communication infrastructure of the Icelandic seismic network (SIL). Each station is connected to a continuously charged car battery to guarantee continuous data collection in case of a power outage.

The monuments of the new GPS stations are identical to conventional CGPS monuments in Iceland, that consist of a 1-m-high short-braced stainless-steel quadripod (Geirsson et al. 2006) as shown in Figure 2. The actual measurement point is a geodetic benchmark drilled/cemented into the ground directly below the center of each quadripod. On Flatey, the bedrock is buried below a 550 m thick sediment layer (Flóvenz & Gunnarsson 1991), so there we used a station setup similar to the short-braced PBO monument, i.e. a central antenna pole is enforced by three slanted stainless-steel poles (Normandeau et al. 2008). The poles were drilled 50 cm into consolidated sediments and welded together 1 m above the surface. We use Septentrio PolaNt antennas without radomes and PolarRx2e receivers for all stations (Table 1). Due to limited vegetation and smooth terrain near most of the stations the sight to orbiting satellites is mostly unhindered. Only at SIFJ (in a fjord) and at GRAN (on a slope) is the satellite view limited until 30° to the East and to the West, respectively.

4.2 GPS Data Processing

The GPS data are sampled every 15 s and stored locally in 24-hr-files. These files are downloaded on a daily basis and then converted to the standard RINEX format. The data are processed with Bernese V5.0 software (Dach et al. 2007) using the final satellite orbits from the Center of Orbit Determination in Europe (CODE), antenna and receiver codes according to the IGS conventions[†] and the standard Bernese routine RNX2SNX. We included 15 IGS stations to tie the daily solutions of the TFZ network into the ITRF2005 reference frame (Altamimi et al. 2007): REYK in Iceland; NAIN, SCH2, STJO on the east coast of Canada; KELY, THU2, QAQ1 on the west coast of Greenland; NYA1 on Spitsbergen and BRUS, MAR6, METS, MORP, KIRU, TRO1, and ONSA in Northern Europe. In addition, we also included five more unconstrained stations in Iceland (BUDH, HEID, ISAK, NYLA, VOGS, Fig. 1). Thus, the data of a total of 34 GPS stations covering a time span of slightly over 4.3 years were included in the processing (2006.7-2011.0).

4.3 CGPS Time Series and Site Velocities

The east, north and vertical velocity components and uncertainties in ITRF05 reference frame were transformed into a fixed North America reference frame using Euler rotation poles from the MORVEL plate model (DeMets et al. 2010) (Table 1). Figure 3 shows the time series for all CGPS stations in North Iceland. The data gaps in the beginning of the times series are mainly due to initial power outage or data transmission problems. Offsets of known events such as earthquakes or antenna changes were identified and corrected for. The antenna of FTEY was replaced in August 2008 (Tab. 1, gray bar in Figure 3) while the antenna of REYK was replaced in March and September 2007. The May 2008 earthquake sequence near Hveragerði in Southwest Iceland included two M6 events, located 50 km east of Reykjavík (Decriem et al. 2010) and caused an additional off-

[†] `http://igscb.jpl.nasa.gov/igscb/station/general/rcvr_ant.tab`

set on the REYK station. All available data since summer 2006 were used for the analysis. The semi-permanent station HEID has only recorded for two 120-day-long periods in 2006 and 2009.

We estimate the velocity of each station following Geirsson et al. (2006): We apply a standard weighted least square approach and describe the daily position $y(t)$ at time t (in years):

$$y(t) = a + bt + A\cos(2\pi t + \phi), \tag{1}$$

where $a+bt$ represents a linear velocity that is modified with an annual oscillation term $A\cos(2\pi t+\phi)$ with a phase offset ϕ and an amplitude A. Outliers were removed individually for each station/component in two stages: (1) All data points with a standard error three times larger than the mean error were dismissed, which eliminated only a couple of points at a few stations. After a first weighted least square fit, (2) all data points with a misfit three times larger than the mean misfit were excluded. On average, this condition excluded 3.4% of the data. Using only the remaining data points, a second weighted least square fit was performed for each single station and component. By estimating each velocity at a time, we assume that the velocities are independent and neglect the slight correlation of daily positions. The variance of the resulting velocities was estimated following Geirsson et al. (2006) by

$$\sigma^2 = \frac{1}{T^2} \cdot \frac{\sum_{i=1}^{N} |y_i - \hat{y}_i|^2}{N - M}, \tag{2}$$

with y_i the i^{th} sample of a total of N data samples, $\hat{y}_i$ the estimated position from $y(t)$ in Eq. (1) and a total of M model parameters. In our case, $M \geq 4$, depending on the number of offsets due to antenna changes, or earthquakes. The $1/T^2$-term scales the velocity uncertainties with an increasing total record time T (Mao et al. 1999).

The formal error of each station position as calculated by the Bernese software is underersti-mated (Dach et al. 2007). This can be demonstrated by the normalized χ^2-value,

$$\chi_n^2 = \frac{1}{N - M} \sum_{i=1}^{N} \frac{|y_i - \hat{y}_i|^2}{\sigma_{B,i}^2}, \tag{3}$$

where $\sigma_{B,i}$ is the formal error for each data point and the other variables as explained above. This equation is normally used to assess the balance between the number of model parameters and the quality of the data fit and is expected to result in a value close to 1. Hence, χ^2_n-values indicate how well the uncertainties correspond to the overall data noise and imply that the BERNESE formal error σ_B is on average 5, 4, and 4 times too small for the east, north and up component, respectively. However, this fact does neither influence the outlier elimination nor the weighted least square fit of the data and the velocity error estimation, since each component is treated individually and the formal error is underestimated by the same factor for all data points.

Figure 4 shows the resulting horizontal and vertical GPS velocities for the North Iceland stations relative to stable North America. The east velocity gradually increases from AKUR (on the North American plate) towards RHOF (on the Eurasian plate). The predicted MORVEL velocity for RHOF – a station that is supposed to be on rigid Eurasian plate – is slightly higher than what we measure. Similar discrepancy is seen at station AKUR, where the MORVEL model predicts a velocity equal to zero, but our measurements indicate a motion towards northwest. However, the amplitude of the total extension between AKUR and RHOF corresponds to the predicted MORVEL extension. Surprisingly, stations on the North American plate (AKUR, SIFJ, GRAN) move in a northwestern direction, away from the boundary zone, which could for example indicate a compression inside the North American plate or a local error in the reference frame. This velocity pattern was also reported by Árnadóttir et al. (2009) and Geirsson et al. (2010). All stations display an uplift up to 5.2 mm/yr (GRAN) except SIFJ and GMEY, the stations furthest away from the fissure swarms. The strongest uplift is seen at GRAN, AKUR and SAVI with diminishing uplift when crossing the fault zones onto the Eurasian plate. This uplift could be due to glacial rebound as suggested by Árnadóttir et al. (2009).

The stations north of Húsavík, on the Tjörnes peninsula, (HEDI, KVIS, HOTJ, ARHO) show a northward motion decreasing with distance from the fault and an eastward motion increasing with distance from the fault. Since the motion on the HFF is mostly of a right-lateral strike-slip type, this pattern must be caused by an additional deformation process. A rotating block between HFF and GOR might be one possibility, but the fact that the stations close to HFF (HEDI/FTEY) show a similar velocity as well as stations close to GOR (ARHO/GMEY) does not support such block rotation. On the other hand, ENVISAT interferograms confirm a circular uplift at Theistareykir central volcano during the observation period, reaching a maximum uplift of 3 cm between the summers of 2007 and 2008 (Fig. 5A and D). This uplift also influences the closest stations, i.e. GRAN, SAVI and the stations on the Tjörnes peninsula.

Figure 6 displays the fault-parallel (N118°E) and -perpendicular (N28°E) velocities for a selection of stations that lie on a profile across the HFF and GOR. The fault-parallel (strike-slip) component of the GPS data accommodates most of the expected plate motion between North America and Eurasia ($\sim$18 mm/yr between AKUR and RHOF). When approaching the HFF from the North American side (AKUR-GRAN-SAVI), the amount of fault parallel velocity slightly decreases instead of increases. This can also be explained with the uplift at Theistareykir volcano, that pushes particularly the stations GRAN and SAVI (and also KVIS and HEDI) to the Northwest (in Fig. 6: negative). Consequently the velocities of stations on the other side of the HFF (HEDI/KVIS/HOTJ/ARHO) increase in linear fashion and finally, the velocity of KOSK and RHOF, north of GOR and on the Eurasian side of the plate boundary, are almost equal. The fault motion of HFF includes also a slight fault-perpendicular (opening) component with the maximum value of 2.5 mm/yr between the stations GRAN and HEDI.

5 MODELING

With an appropriate model that describes the observations of the TFZ transform motion we are able to estimate the amount of moment that has been accumulated on the fault segments and could be unleashed in a potential major future earthquake. We describe the surface deformation of the TFZ with a back slip model consisting of planar dislocations in an elastic half space and an inflating Mogi source representing the uplift of the Theistareykir central volcano, using the CGPS velocities as input data. To constrain the location of the Mogi source we used InSAR data. Due to lack of data to create an InSAR time-series, we use GPS data only for the final (combined back slip and Mogi) model. The resulting best fit model parameters include the locking depth and indicate the slip deficit rate on the HFF, which can be used to estimate the seismic moment that has accumulated since the last big event in 1872.

5.1 TFZ Back Slip Model

Interseismic deformation at plate boundaries is commonly described by the relative motion of two elastic blocks that are tightly connected (*locked*) to one another down to a certain depth (*locking depth*) but move at full plate rate below that depth. Hence, in a fault-fixed reference frame the model predicts full plate velocities in the far-field, which decrease and finally become zero (no motion) at the boundary itself. Savage & Prescott (1978) described the interseismic velocity field with a uniform strike-slip on a lower section of a vertical fault plane. We modify that model slightly by (1) also allowing for an opening component and (2) using the so-called *back slip concept* (Fig. 7): The continuous motion of two rigid blocks is superposed with a steady back-slip creep on upper part of the discontinuity in opposite direction. Together, these two velocity fields describe an interseismic velocity field from a locked fault.

We simulate the TFZ with a plate boundary model that consists of nine dislocation segments (Fig. 7). All segments move freely below their locking depth, but are fully locked above. One main rifting segment representing the MAR is offset by two parallel transforms in the TFZ that thus bound a small block. This block is defined by segment **A** in the Northeast representing the GOR and segments **B** and **C** in the Southwest expressing the HFF. Segment **D** follows the Eyjarfjarðaráll Rift as well as earthquake locations, and segments **E** and **F** connect the GOR and the HFF to Kolbeinsey Ridge segment **H** in the North. The block is bounded by another auxiliary rift segment **G** on the southeastern side that links to the Northern Volcanic Zone segment **I**. The orientation of the rifting segments (**G**-**I** and **H**-**E**) is more or less perpendicular to the N105°E MORVEL plate motion azimuth. The locations of the GOR and HFF segments follow approximately earthquake locations and, in case of segment **C**, the fault surface trace.

Each segment is described by ten parameters: Seven parameters define the geometry (length, width, depth, strike and dip angle, east/north location) and three parameters indicate the segment displacement (strike-slip, dip-slip and opening). The total number of model parameters is therefore 90 but we make the following assumptions to reduce the number of unknowns: (1) All segments have a dip of 90 degrees. (2) The location and strike of all segments is fixed leaving the locking depth as the only free geometrical parameter. (3) The locking depths were reduced to two, i.e. one for the ridge segments (**G**-**H** and **E**-**I**) and one for the transform segments. (4) The opening and strike-slip of each dislocation is described by the full plate motion, where (5) the full plate motion is distributed on the segments forming a block, and finally (6) no dip-slip is allowed. Although HFF and GOR show different fault characteristics (Rögnvaldsson et al. 1998), we decided to describe them in the same way in our model, a simplification we justify with the lack of GPS data to resolve the motion on GOR. As a result, we are left with only five free parameters that describe the whole model: The two locking depths for opening and transform segments, the azimuth and amplitude of the total plate motion and the partial motion of the HFF segment, which at the same time defines the motion on the GOR and of the segments bounding the block. We then add two additional parameters to correct for the possible reference frame shift of 6-7 mm/yr that seems to affect the velocities of all stations.

5.2 Modeling the uplift at Theistareykir volcano

ENVISAT interferograms between 2005 and 2009 show a circular uplift signal coinciding with the Theistareykir central volcano with a maximum deformation rate between 2007 and 2008, affecting GPS velocities of stations in its vicinity. We model the deformation with an expanding Mogi source in an elastic half-space and use the two best interferograms covering the time span 2007-2008 as input data to constrain the location and depth of the inflation source.

The key parameters of the two ascending and descending ENVISAT interferograms are given in Table 2. They were processed with the GAMMA software using a digitized elevation model that was generated by the Icelandic Meteorological Office (IMO) and updated with three ERS-1/2 tandem interferograms. A plane was removed to correct for possible orbital errors and the deformation signal was also normalized to the same time span. The resulting interferograms are of different quality, with the descending interferogram (Fig. 5D) exhibiting strong atmospheric variations, while the ascending interferogram is relatively free of atmospheric disturbances. However, both interferograms show a line-of-sight uplift rate of $\sim$3 cm/yr. The number of InSAR data points was reduced by quadtree sub-sampling, where each interferogram is subdivided into squares of different size, depending on the data variance of each cell (Jónsson et al. 2002). Areas with uniform data are represented by larger cells whereas areas with high variance are subdivided into smaller cells. The benefit of this sub-sampling procedure is to reduce the amount of data without losing details of the deformation signal. The Mogi model parameter optimization approach is the same as for the interseismic model and is explained in the following section.

Despite the low quality of the descending scene we were able to constrain well the location of the Mogi source south of Tjörnes peninsula and below the Theistareykir central volcano at 8.5 km depth. The source depth implies that the uplift is caused by magmatic pressure increase. Having constrained the location of the Mogi source, we then add the Mogi model to our back slip model to predict the measured GPS velocities (Fig. 7). The model represents the data of the ascending scene very well but of course cannot account for the atmospheric variations of the descending scene (Fig. 5).

The resulting surface deformation at the GPS stations derived from the Mogi model (assuming constant deformation rate during 2006-2010) is listed in Table 3. The largest deformation is expected at station SAVI (3.6 mm/yr towards west, 4.5 mm/yr in radial direction), but unfortunately the time series of that station does not cover the time before, during and after the period of maximum inflation rate (Fig. 3, green boxes). Station GRAN, affected by the modeled inflation by 2.9 mm/yr towards west, is the only station where a transient signal is visible. Otherwise, the influence of the Mogi deformation is hardly above the noise level and GPS time series do not reveal any clearly visible transients. We therefore assume a constant inflation rate over the time span of the GPS data acquisition.

5.3 Optimization approach

We can reproduce the observed GPS velocities with our combined interseismic and Mogi model using the best fit parameters that are found using a two-step optimization routine: First, a Monte-Carlo type, simulated annealing process scans the whole model space for the trough containing the global minimum (e.g. Cervelli et al. 2001). The range of values that define the model space is listed in Table 4. This procedure picks at first random combinations of model parameters but then gradually favors parameter combinations with a low misfit, as has been described by Metropolis et al. (1953) and Creutz (1980). Then, a second, derivative based optimization routine uses the optimal solution from the simulated annealing process as a starting point to find the best fit solution within the identified global minimum trough. We run this two-step optimization procedure several times to verify the reproducibility of our results. All input GPS data points are weighted with their corresponding uncertainties as they have been derived from Eq. (2). The GPS velocities and the best model fit are shown in Figure 8 and the best solution for each parameter in Tab. 4.

We estimate the uncertainties of the best fit model parameters using the following method: We add Gaussian random noise to the input GPS velocities, $v_i' = v_i + \Delta v_i$, which corresponds to their velocity uncertainty σ_i, and repeat the optimization, getting a new best fit solution. After 1000 runs with iteratively modified input data, we can statistically estimate the uncertainty for each model parameter. By doing so, we can propagate the error of the input data through the model, but the obtained uncertainties do not reflect the uncertainty of the underlying model itself. Figure 9 shows the distribution of resulting parameters with modified input data.

5.4 Modeling Results

We find a locking depth of $6.7^{+1.8}_{-1.3}$ km for the transform fault segments and $7.2^{+1.6}_{-1.4}$ km for the ridge segments. The total spreading motion between the North American an the Eurasian plate results in $20.1^{+0.8}_{-0.7}$ mm/yr with an azimuth of N112°E±2°. The partial motion accommodated by HFF is estimated with 34±3% of the total motion and the volume change rate of the inflating Mogi source is found to be $10.0^{+1.2}_{-1.0}{\cdot}10^6$ m^3/yr. All optimal model parameters are well within the given bounds of the model parameter search space and show no obvious correlation (Fig. 9). We also used cross validation to evaluate how well the model parameters are constrained and it resulted in somewhat smaller parameter uncertainties than the outcome obtained by the error estimation described above.

The results indicate a mean fault slip rate of 6.8±0.7 mm/yr on the offshore and 6.7±0.7 mm/yr on the onshore HFF segment. If we assume a steady slip rate and that the HFF has been locked since the last big earthquake in 1872, then the accumulated slip deficit is 0.83-1.05 m. We can then calculate the accumulated seismic moment M_0 using

$$M_0 = \mu A u, \tag{4}$$

with μ =30 GPa being the shear modulus, A the total potential rupture area along the 110 km long fault segments **B** and **C** (Fig. 7) and u the average slip deficit. From this we can estimate the moment magnitude M_w (in Nm),

$$M_w = \frac{2}{3} \log_{10} M_0 - 6.03 \tag{5}$$

as it has been derived from Hanks & Kanamori (1979). Thus, if all accumulated moment since the last big event would be released in one large earthquake on the HFF, its moment magnitude could reach $M_w = 6.8 \pm 0.1$.

6 DISCUSSION

The locking depth we estimate of $6.7^{+1.8}_{-1.3}$ km is shallower than previous estimates for the locking depth on the HFF, except that by Árnadóttir et al. (2009). First locking depth estimations were indirectly inferred by Rögnvaldsson et al. (1998) after relocating nearly 900 earthquakes in 60 earthquake swarms between 1994-1998 in the TFZ: The number of earthquakes decayed dramatically below 8 km of depth and only 10% of the earthquakes occurred below 10 km, with the deepest earthquakes at 16 km and a maximum uncertainty of 2 km. Their result is mainly driven by earthquake swarms west of the island Flatey, whereas our estimation is controlled by GPS measurements at the eastern end of the HFF. Also, earthquake locations of events outside a seismic network (as it was the case for some of these earthquake swarms) might be biased. However, a possible explanation for this discrepancy would be that the locking depth decreases from the northwestern end of the fault towards the NVZ. Jouanne et al. (2006) found a GPS station velocity difference of ∼8 mm/yr across the HFF between points close to the stations GRAN and KVIS and concluded that the locking depth must be slightly larger than the 10 km, a claim that was in part based on the results of Rögnvaldsson et al. (1998), which again is significantly deeper than our estimate.

The magnitude estimation of the accumulated moment along the HFF of $M_w = 6.8 \pm 0.1$ is based on four assumptions: (1) Complete stress relaxation by the 1872 $M_w = 6.5$ earthquakes and steady stress accumulation since then, (2) uniform slip rate and a constant locking depth, (3) a rupture along the whole total fault plane with a dimension constrained by the locking depth and (4) the fault model length, which is the sum of the segments **B** and **C** in Figure 7. In fact, the onshore segment **C** ends within the Theistareykir fissure swarm and is ~18 km shorter than the model segment. Using Equation (4) and (5) with the adapted length reduces the magnitude estimation only within the rounding precision. Also, the stress accumulation on HFF might have been influenced by the Krafla rifting episode 1975-1984 that appears to have reduced the seismicity on the eastern end of the fault (Rögnvaldsson et al. 1998). Another fact that might be taken into account to estimate the potential devastating energy would be the direction of rupture. If this potential event would initiate at the northwestern end of the fault, the rupture would propagate *towards* Húsavík and the surrounding farms, which causing a superposition and thus enhancement of the surface waves.

The initial estimation for the partial motion of HFF of 40% from Geirsson et al. (2006) is somewhat higher than our result (34±3%), but their estimate was based on only three continuous GPS stations. However, all the above observations indicate that HFF as well as GOR accommodate the total transform motion within the TFZ. In our model we do not account for a possible active Dalvík lineament (Figure 1). The GPS velocities 2006-2010 as well as the lack of micro seismicity do not support the presence of an active Dalvík lineament. On the contrary, stations northeast of the lineament (e.g. GRAN/SAVI) show a larger NE-component than AKUR, which is located on the other side of the lineament. However, the continuous GPS data points close to the lineament are too sparse to provide detailed information about a possible active Dalvík lineament.

The overall spreading rate of $20.1^{+0.8}_{-0.7}$ mm/yr is slightly higher than what the MORVEL model predicts (18 mm/yr) and the azimuth of N112°E is also different than expected from MORVEL (N105°E). In the least square optimization the GPS data were projected on a (flat) UTM model surface. This causes an angular distortion of +1° to +3° and thus explains part of the azimuthal discrepancy between the two models.

7 CONCLUSION

The CGPS time series presented in this paper cover the whole Tjörnes Fracture Zone (150 km by 100 km) in North Iceland expanding the existing network from 4 to 14 stations. The resulting GPS velocities from four years of data show clearly the transform motion in the TFZ and the full plate spreading between the North American and the Eurasian plate. The transform motion is accommodated by the HFF and the GOR in a ratio of 34%/66% with an uncertainty of $\pm$3%. In addition, the GPS velocities show influence from uplift at Theistareykir central volcano, which likely is caused by magma accumulation at $\sim$8.5 km depth. We used a combined back-slip and Mogi source model to describe the surface deformation as seen with the CGPS data, and for the first time key parameters of the kinematics of the Tjörnes Fracture Zone were estimated with uncertainties. We find a shallow locking depth for the Húsavík Flatey fault of $6.8^{+2.3}_{-1.6}$ km and a resulting slip deficit of 0.83-1.05 m. Assuming a steady slip rate since 1872, this slip deficit would correspond to a potential $M_w 6.8\pm0.1$ earthquake. The resulting locking depth is shallower than previous results based on earthquake hypocenter depths. One possible explanation might be the local distribution of the input data: Our model is constrained by GPS points close to the southeastern end of the fault, where as the majority of earthquakes used in previous studies is located at the other end of the fault.

ACKNOWLEDGMENTS

We thank Thóra Árnadóttir who initiated the umbrella project to densify the network of high-rate continuous GPS stations in Iceland supported by the Icelandic Research Fund (grant nr. 060243013). Janik Deutscher, Thorgils Ingvarsson and Judicael Decriem helped to install the stations in North Iceland. The GPS data of the stations AKUR and HEID is courtesy of The National Land Survey of Iceland (LMI). The stations ARHO and RHOF were installed by Thierry Villemin (Laboratoire Géodynamique des Chaînes Alpines, LGCA) and are run by IMO with financial support of the Institut Polaire Paule Emile Victor (IPEV). Thierry Villemin and IMO also granted access to the data. We are grateful to Michael Müller who helped with BERNESE processing. The Húsavík Academic Center allowed us to use their facilities during field work. This work was supported by grants from ETH Zürich and the Icelandic Equipment Fund (grant nr. 061059). ENVISAT data were provided by the European Space Agency through category-1 project #3846. Some figures were produced with the GMT public domain software (Wessel & Smith 1998). We thank an anonymous reviewer and Erik Sturkell for helping to improve the manuscript.

REFERENCES

Alcoa press release, 2006. "Alcoa, Government of Iceland and Municipality of Húsavík Sign Memorandum of Understanding", 17.05.2006, `http://www.alcoa.com/iceland/en/news/whats_new/2006/2006_05_mou.asp`.

Altamimi, Z., Collilieux, X., Legrand, J., Garayt, B., & Boucher, C., 2007. ITRF2005: A new release of the International Terrestrial Reference Frame based on time series of station positions and earth orientation parameters, *J. Geophys. Res.*, **112**(B9).

Árnadóttir, T., Geirsson, H., Hreinsdottir, S., Jónsson, S., LaFemina, P., Bennett, R., Decriem, J., Holland, A., Metzger, S., Sturkell, E., & Villemin, T., 2008. Capturing crustal deformation signals with a new high-rate continuous GPS network in Iceland, *Fall Meet. Suppl., Eos Trans. AGU*, **89**(53), G43A–0650.

Árnadóttir, T., Lund, B., Jiang, W., Geirsson, H., Björnsson, H., Einarsson, P., & Sigurdsson, T., 2009. Glacial rebound and plate spreading: results from the first countrywide GPS observations in Iceland, *Geophys. J. Int.*, **177**(2), 691–716.

Björnsson, A., 1985. Dynamics of crustal rifting in NE Iceland, *J. Geophys. Res.*, **90**(NB12), 151–162.

Brandsdóttir, B., Riedel, C., Richter, B., Helgadóttir, G., Kjartansson, E., Dahm, T., Detrick, R., Mayer, L., Calder, B., & Driscoll, N., 2005. Multibeam bathymetric maps of the Kolbeinsey Ridge and Tjörnes Fracture Zone, N-Iceland, *EGU General Assembly*, (EGU05), A–07219.

Cervelli, P., Murray, M. H., Segall, P., Aoki, Y., & Kato, T., 2001. Estimating source parameters from deformation data, with an application to the March 1997 earthquake swarm off the Izu Peninsula, Japan, *J. Geophys. Res.*, **106**(B6), 11217–11237.

Creutz, M., 1980. Monte-Carlo study of quantized SU(2) Gauge-theory, *Phys. Rev.*, **21**(8), 2308–2315.

Dach, R., Hugentobler, U., Fridez, P., & Meindl, M., 2007. *Bernese GPS Software Version 5.0*, Stämpfli Publications AG, Bern.

Decriem, J., Árnadóttir, T., Hooper, A., Geirsson, H., Sigmundsson, F., Keiding, M., Ofeigsson, B. G., Hreinsdottir, S., Einarsson, P., LaFemina, P., & Bennett, R. A., 2010. The 2008 May 29 earthquake doublet in SW Iceland, *Geophys. J. Int.*, **181**(2), 1128–1146.

DeMets, C., Gordon, R. G., & Argus, D. F., 2010. Geologically current plate motions, *Geophys. J. Int.*, **181**(1), 1–80.

Einarsson, P., 1991. Earthquakes and present-day tectonism in Iceland, *Tectonophysics*, **189**(1-4), 261–279.

Einarsson, P., 2008. Plate boundaries, rifts and transforms in Iceland, *Jökull*, **58**, 35–58.

Flóvenz, O. G. & Gunnarsson, K., 1991. Seismic crustal structure in Iceland and surrounding area, *Tectonophysics*, **189**(1-4), 1–17.

Foulger, G. R., Jahn, C. H., Seeber, G., Einarsson, P., Julian, B. R., & Heki, K., 1992. Post-rifting stress-relaxation at the divergent plate boundary in Northeast Iceland, *Nature*, **358**(6386), 488–490.

Geirsson, H., Árnadóttir, T., Völksen, C., Jiang, W., Sturkell, E., Villemin, T., Einarsson, P., Sigmundsson, F., & Stefansson, R., 2006. Current plate movements across the Mid-Atlantic Ridge determined from 5 years of continuous GPS measurements in Iceland, *J. Geophys. Res.*, **111**(B9).

Geirsson, H., Árnadóttir, T., Hreinsdóttir, S., Decriem, J., LaFemina, P. C., Jónsson, S., Bennett, R. A., Metzger, S., Holland, A., Sturkell, E., Villemin, T., Völksen, C., Sigmundsson, F., Einarsson, P., Roberts, M., & Sveinbjörnsson, H., 2010. Overview of results from continuous GPS observations in Iceland from 1995 to 2010, *Jökull*, **60**, 3–22.

Grönvold, K., 2011. Institute of Earth Sciences, University of Iceland, Reykjavik.

Hanks, T. C. & Kanamori, H., 1979. Moment magnitude scale, *J. Geophys. Res.*, **84**(NB5), 2348–2350.

Heki, K., Foulger, G. R., Julian, B. R., & Jahn, C. H., 1993. Plate dynamics near divergent boundaries - geophysical implications of postrifting crustal deformation in NE Iceland, *J. Geophys. Res.*, **98**(B8), 14279–14297.

Hofton, M. A. & Foulger, G. R., 1996. Postrifting anelastic deformation around the spreading plate boundary, North Iceland. 1. Modeling of the 1987-1992 deformation field using a viscoelastic earth structure, *J. Geophys. Res.*, **101**(B11), 25403–25421.

Hönnun engineering consultants, 2005. Primary aluminum plant located near Húsavík, Site study, `http://www.hrv.is/media/files/Husavik_site\%20report_web.pdf`.

Jónsson, S., Zebker, H., Segall, P., & Amelung, F., 2002. Fault slip distribution of the 1999 M_w 7.1 Hector Mine, California, earthquake, estimated from satellite radar and GPS measurements, *Bull. Seismol. Soc. Amer.*, **92**(4), 1377–1389.

Jouanne, F., Villemin, T., Ferber, V., Maveyraud, C., Ammann, J., Henriot, O., & Got, J. L., 1999. Seismic risk at the rift-transform junction in north Iceland, *Geophys. Res. Lett.*, **26**(24), 3689–3692.

Jouanne, F., Villemin, T., Berger, A., & Henriot, O., 2006. Rift-transform junction in North Iceland: rigid blocks and narrow accommodation zones revealed by GPS 1997-1999-2002, *Geophys. J. Int.*, **167**(3), 1439–1446.

Långbacka, B. O. & Gudmundsson, A., 1995. Extensional tectonics in the vicinity of a transform-fault in North Iceland, *Tectonics*, **14**(2), 294–306.

Mao, A. L., Harrison, C. G. A., & Dixon, T. H., 1999. Noise in GPS coordinate time series, *J. Geophys.*

Res., **104**(B2), 2797–2816.

McMaster, R. L., Schilling, J. G. E., & Pinet, P. R., 1977. Plate boundary within Tjörnes Fracture Zone on northern Icelands insular margin, *Nature*, **269**(5630), 663–668.

Metropolis, N., Rosenbluth, A. W., Rosenbluth, M. N., Teller, A. H., & Teller, E., 1953. Equation of state calculations by fast computing machines, *J. Chem. Phys.*, **21**(6), 1087–1092.

Normandeau, J., Meertens, C., & Bartel, B., 2008. GPS antenna monuments and mounts supported by UNAVCO: Options and Effectiveness, *Eos Trans. AGU*, **89**(53), Fall Meeting Suppl., Abstract G41B–0627.

Rögnvaldsson, S. T., Gudmundsson, A., & Slunga, R., 1998. Seismotectonic analysis of the Tjörnes Fracture Zone, an active transform fault in north Iceland, *J. Geophys. Res.*, **103**(B12), 30117–30129.

Savage, J. C. & Prescott, W. H., 1978. Astenosphere readjustment and earthquake cycle, *J. Geophys. Res.*, **83**(NB7), 3369–3376.

SIL, 2008. A selection of earthquakes of the Seismic In Iceland (SIL) catalogue, `http://hraun.vedur.is/ja/ymislegt/storskjalf.html`.

Stefánsson, R., 1979. Catastrophic earthquakes in Iceland, *Tectonophysics*, **53**(3-4), 273–278.

Stefánsson, R., Gudmundsson, G. B., & Halldórsson, P., 2008. Tjörnes fracture zone. New and old seismic evidences for the link between the North Iceland rift zone and the Mid-Atlantic ridge, *Tectonophysics*, **447**(1-4), 117–126.

Tryggvason, E., 1973. Seismicity, earthquake swarms, and plate boundaries in the Iceland region, *Bull. Seismol. Soc. Amer.*, **63**(4), 1327–1348.

Tryggvason, E., 1980. Subsidence events in the Krafla area, North-Iceland, 1975-1979, *J. of Geophys.*, **47**(1-3), 141–153.

Tryggvason, E., 1984. Widening of the Krafla fissure swarm during the 1975-1981 volcano-tectonic episode, *Bull. of Volc.*, **47**, 47–69.

Völksen, C., 2000. *Die Nutzung von GPS für die Deformationsanalyse in regionalen Netzen am Beispiel Islands*, Ph.D. thesis, Wissenschaftliche Arbeiten der Fachrichtung Vermessungswesen, Universität Hannover.

Wesnousky, S. G., 1986. Earthquakes, quaternary faults, and seismic hazard in California, *J. Geophys. Res.*, **91**(B12), 2587–2631.

Wessel, P. & Smith, H. F., 1998. New improved version of the Generic Mapping Tools released, in *EOS Trans. Am. Geophys. Un.*, vol. 79.

Table 1. Station information with the velocities given in mm/yr relative to stable North America. LMI: National Land Survey of Iceland, IMO: Icelandic Meteorological Office, LGCA: Laboratoires de Géodynamique des Chaînes Alpines, ETH: Swiss Federal Institute of Technology.

Station	Latitude	Longitude	Antenna	Receiver	Since	Agencies	v_{E}	v_{N}	v_{U}
AKUR	65.6854	-18.1225	TRM29659.00	TRIMBLE 4700	2001	LMI	-5.0±0.4	2.8±0.3	4.7±1.2
ARHO	66.1931	-17.1090	ASH701945C_M	ASHTECH UZ-12	2002	IMO/LGCA	2.1±0.3	-0.3±0.3	0.5±0.9
FTEY	66.1603	-17.8479	TRM41249.00	TRIMBLE NETRS	2007.6	IMO/ETH	-1.6±0.3	2.2±0.4	1.6±1.4
			AERAT2775_43	SEPT POLARX2	2008.7				
GAKE	66.0781	-16.7647	AERAT2775_43	SEPT POLARX2	2006.9	IMO/ETH	6.2±0.3	0.3±0.4	3.2±1.4
GMEY	66.5390	-18.0190	AERAT2775_43	SEPT POLARX2	2007.0	IMO/ETH	1.3±0.3	-1.1±0.3	-1.1±1.5
GRAN	65.9187	-17.5786	AERAT2775_43	SEPT POLARX2	2006.7	IMO/ETH	-6.8±0.5	2.7±0.3	5.2±1.5
HEDI	66.0807	-17.3094	AERAT2775_43	SEPT POLARX2	2006.9	IMO/ETH	-1.8±0.4	2.7±0.3	2.1±1.3
HEID	65.3808	-14.5409	TRM41249.00	TRIMBLE 5700	2006.6	LMI	12.7±0.4	-6.3±0.4	5.1±1.3
			TRM55971.00	TRIMBLE NETR5	2009.6				
HOTJ	66.1617	-17.2443	AERAT2775_43	SEPT POLARX2	2006.9	IMO/ETH	0.6±0.3	0.6±0.3	0.9±1.4
KOSK	66.3033	-16.4434	AERAT2775_43	SEPT POLARX2	2006.9	IMO/ETH	10.0±0.5	-4.7±0.6	2.5±1.3
KVIS	66.1008	-17.2717	AERAT2775_43	SEPT POLARX2	2006.8	IMO/ETH	-1.1±0.4	1.5±0.3	1.9±1.3
RHOF	66.4611	-15.9467	ASH701945C_M	ASHTECH UZ-12	2001	IMO/LGCA	11.1±0.2	-5.1±0.2	0.7±0.9
SAVI	65.9932	-17.3761	AERAT2775_43	SEPT POLARX2	2007.6	IMO/ETH	-6.2±0.5	3.0±0.4	4.1±1.5
SIFJ	66.1380	-18.8993	AERAT2775_43	SEPT POLARX2	2006.7	IMO/ETH	-4.7±0.4	0.5±0.3	-1.5±1.3

Table 2. Key parameters of the two interferograms used to model the inflation at Theistareykir central volcano, including temporal (ΔT) and perpendicular baseline ($B_\perp$).

Pass	Track	Frame	Acquisition dates	ΔT	$B_\perp$
Asc.	230	1323	20070627-20080611	350 d	10 m
Des.	281	2277	20070701-20080824	419 d	370 m

Table 3. Effect of the Theistareykir uplift at GPS receivers using an inflating Mogi source located at 65.88734°N and 17.00733°W and the volume change rate that is given in Table 4.

Station	Radial distance	Deformation rate [mm/yr] Up	Radial	East	North
SAVI	20.3 km	1.9	4.5	-3.6	2.7
GAKE	23.6 km	1.3	3.6	1.7	3.1
HEDI	25.2 km	1.1	3.2	-1.6	2.7
GRAN	26.2 km	1.0	3.0	-2.9	0.5
KVIS	26.3 km	1.0	3.0	-1.3	2.7
HOTJ	32.0 km	0.6	2.1	-0.6	2.0
ARHO	34.0 km	0.5	1.9	-0.2	1.9
FTEY	48.5 km	0.2	1.0	-0.7	0.6
KOSK	52.6 km	0.1	0.8	0.4	0.7
AKUR	55.9 km	0.1	0.7	-0.7	-0.3
RHOF	79.5 km	0.0	0.4	0.2	0.3
GMEY	85.4 km	0.0	0.3	-0.2	0.3
SIFJ	90.1 km	0.0	0.3	-0.3	0.1
HEID	127.0 km	0.0	0.2	0.2	-0.0

Table 4. Best fit model solutions

Model parameter	Best fit	Search range	Unit
Locking depth HFF/GOR	$6.7^{+1.8}_{-1.3}$	1-15	km
Locking depth Ridge	$7.2^{+1.6}_{-1.4}$	1-15	km
Total opening motion	$20.1^{+0.8}_{-0.7}$	18-28	mm/yr
Azimuth of motion	114.5 ± 1.5	105-120	N°E
Partial motion on HFF	34 ± 3	10-60	%
Mogi volume change rate	$10.0^{+1.2}_{-1.0}$	0-20	$\cdot10^6$ m^3/yr

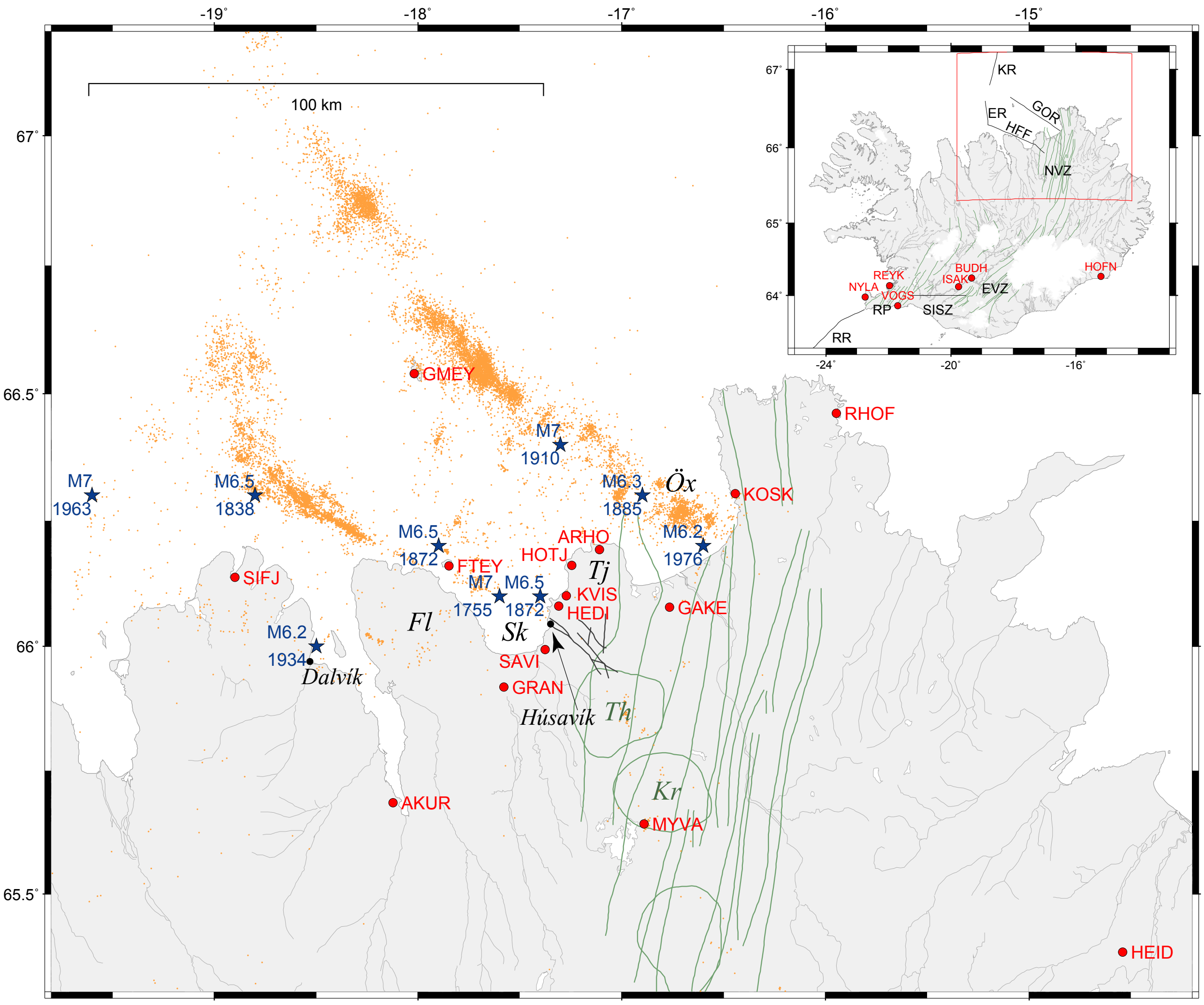

Figure 1. Tectonic setting, seismicity and GPS stations in (North) Iceland. The Mid-Atlantic Ridge is offset by the South Icelandic Seismic Zone in the South (SISZ) and by the Húsavík Flatey Fault (HFF) and the Grímsey Lineament (GOR) in the North (inset). Large historical earthquakes with given magnitude and year are marked with blue stars (after Stefánsson et al. 2008). Orange dots show the M>2 earthquake locations 1992-2008 (after SIL 2008). The surface fault traces of the HFF in the Húsavík area are plotted as dark gray lines (after Rögnvaldsson et al. 1998). Fissure swarms are indicated with green lines. Central volcanoes: Th – Theistareykir, Kr – Krafla. Other plate boundary segments: RR – Reykjanes Ridge, RP – Reykjanes Peninsula, EVZ – Eastern Volcanic Zone, NVZ – Northern Volcanic Zone, ER – Eyjarfjarðaráll Rift, KR – Kolbeinsey Ridge. Other features: Fl – Flateyjarskagi peninsula, Sk – Skjálfandi bay, Tj – Tjörnes peninsula, Öx – Öxarfjörður bay.

Figure 2. Example of a set up for the continuous GPS stations in North Iceland. The stainless-steel quadripod of the station SAVI is drilled and cemented into the ground. The box protects the GPS receiver and the wireless LAN antenna, which is used for data transmission to an Internet access in 6 km aerial distance.

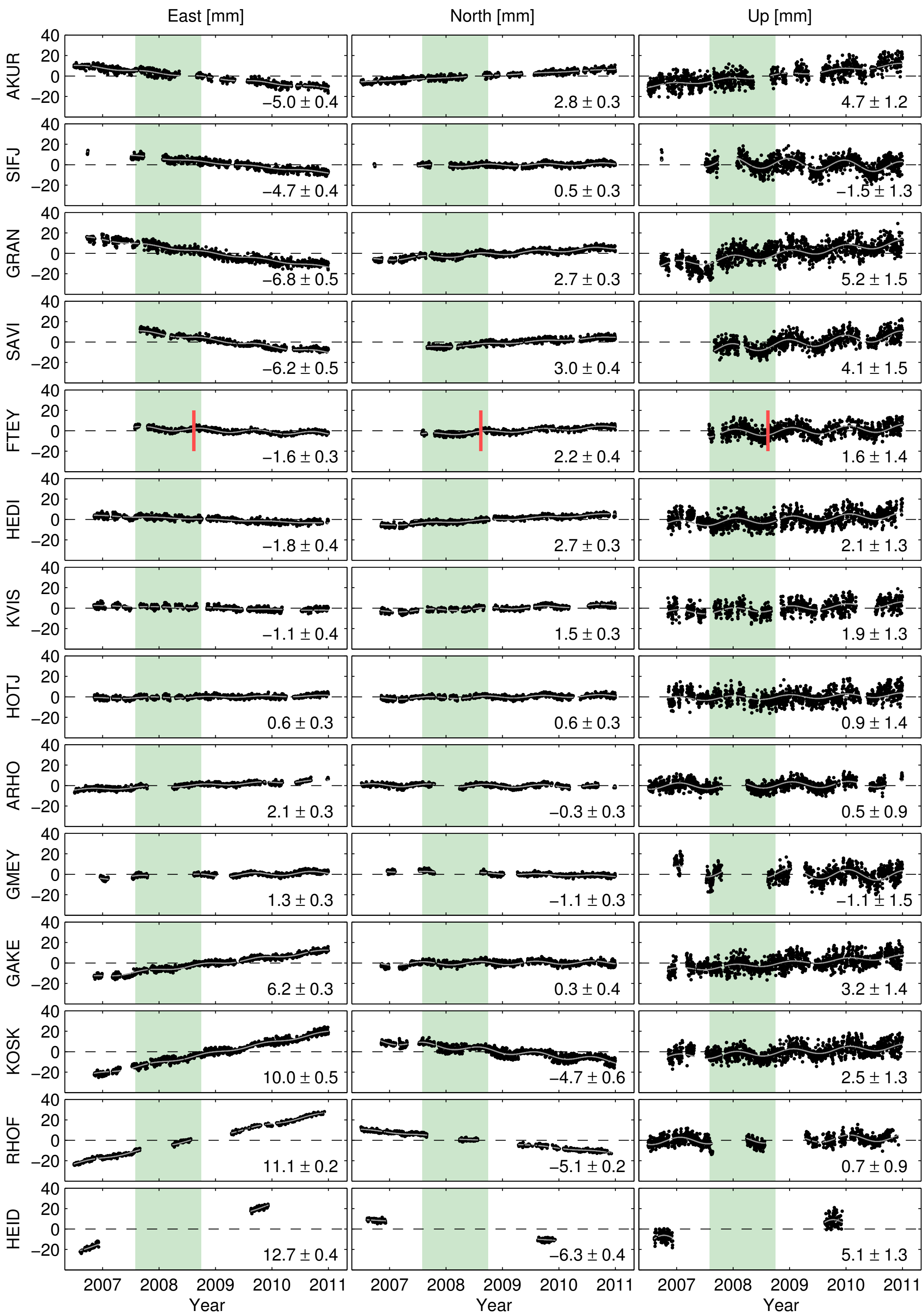

Figure 3. Time series from the continuous stations in North Iceland displaying the east, north and up components. The data are offset corrected (red bar at station FTEY), with outliers removed, displayed relative to stable North America and arranged from North American (top) to Eurasian plate (bottom). The gray lines display the best data fit using Eq. (1). The velocities and uncertainties are given in mm/yr. The light green area marks the period of maximum uplift rate at Theistareykir central volcano.

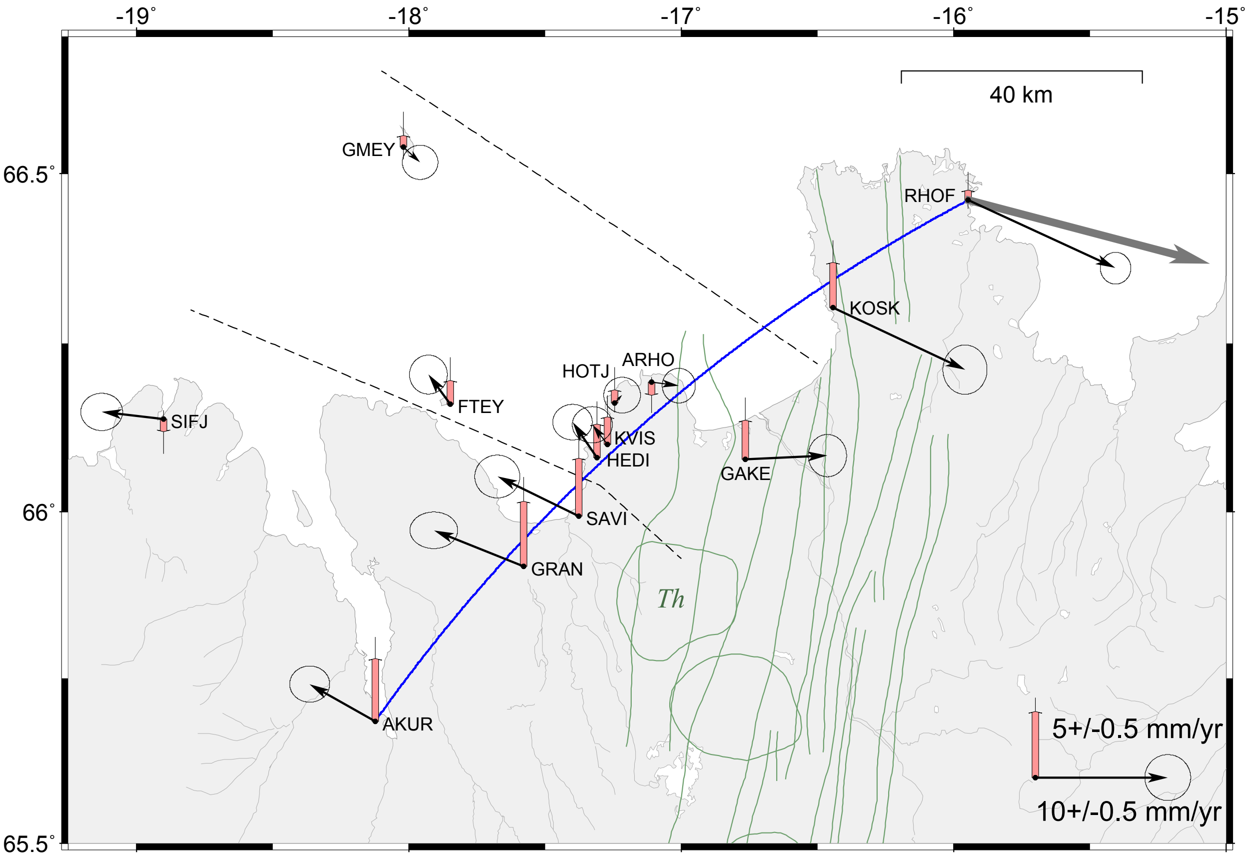

Figure 4. Horizontal (black, 95% confidence level) and vertical (red, 68% confidence level) GPS velocities, relative to stable North America. Fault segments of HFF and GOR (dashed lines), fissure swarms with the corresponding central volcanoes (green lines) and the MORVEL value for RHOF (gray arrow) are indicated. The locations along the blue curve were used for the modeled velocities in Figure 6. Th - Theistareykir central volcano.

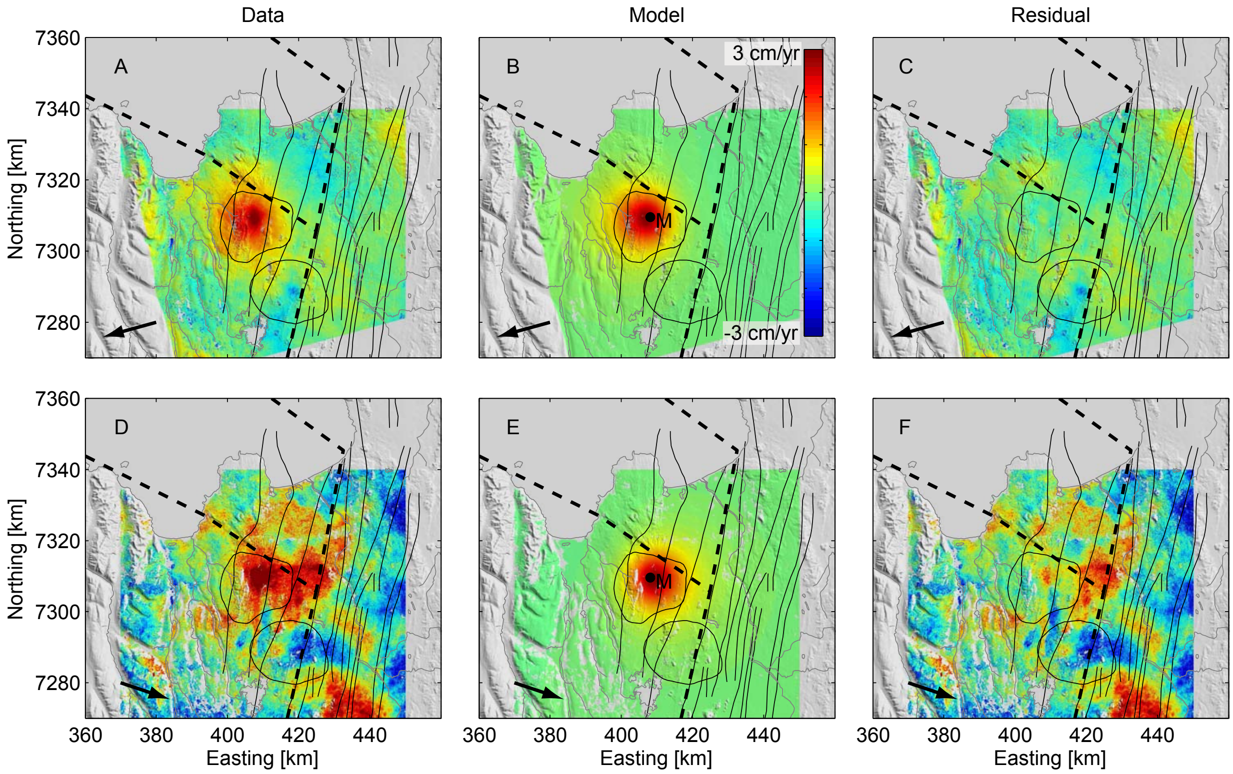

Figure 5. Unwrapped ENVISAT interferograms spanning 2007-2008, with the deformation normalized to one year (A/D), Mogi model prediction with the Mogi source **M** indicated (B/E), and residuals between the data and the model predictions (C/F) for ascending (A-C) and descending track (D-F). The dashed lines mark the model segments of the plate-boundary and the arrows indicate the line-of-sight (LOS) from the ground towards the satellite.

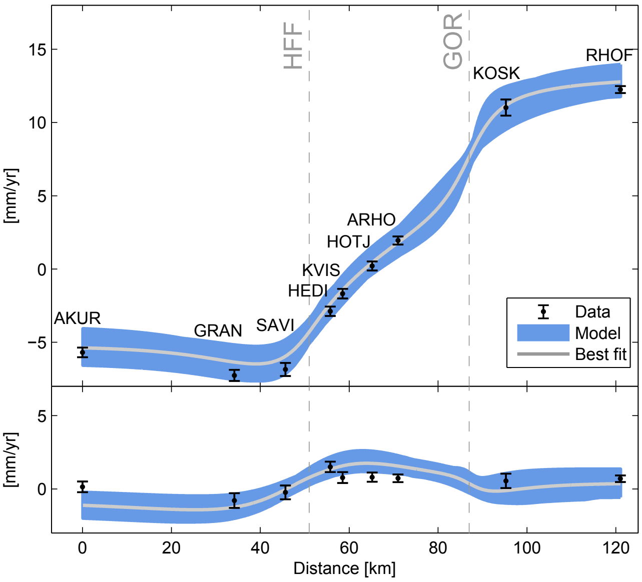

Figure 6. Velocity profiles across the HFF for fault parallel (above) and perpendicular velocities (below). The data (black) of the stations along the AKUR-RHOF-profile (Fig. 4) are shown with 68%-confidence level. The blue area marks the upper and lower boundary of the best fit (gray line) that results from the error estimation for a curved profile between AKUR and RHOF (Fig. 4).

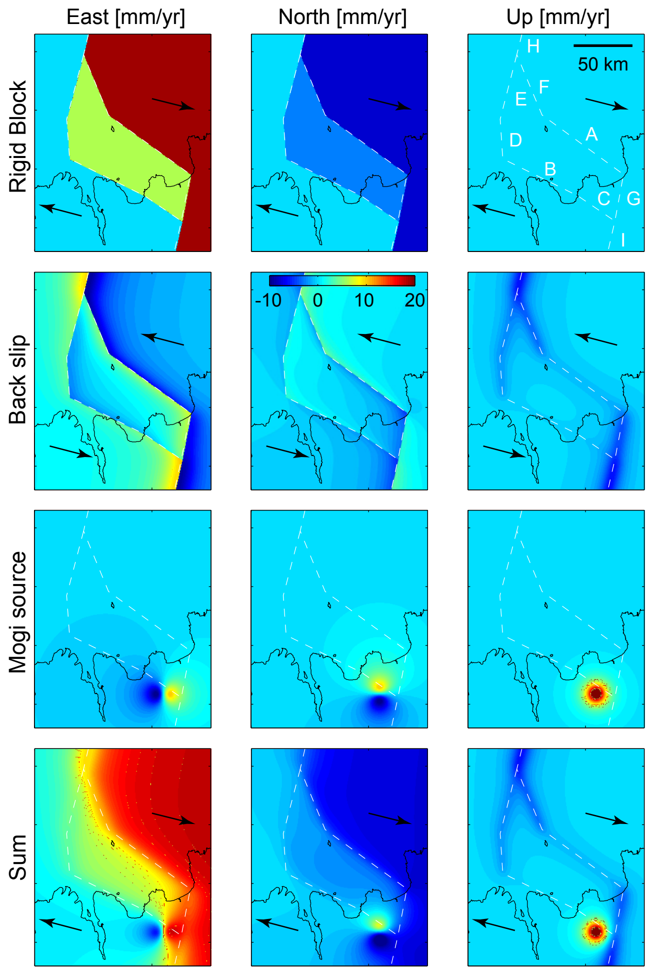

Figure 7. The three columns show the surface deformation velocities for east, north and up component: The back slip concept is based on the superposition of two moving, rigid blocks (1st row) and reverse back slip of the locked part of the plate boundary (2nd row). An inflating Mogi source accounts for the local deformation at Theistareykir central volcano (3rd row). Altogether they build the surface deformation model for the Tjörnes Fracture Zone used in this study. The model dislocation segments **A** to **G** bound a tectonic block between the North American and the Eurasian plate. Black arrows symbolize the main motion direction. The color scale indicates the velocities for each component [mm/yr] w.r.t North America.

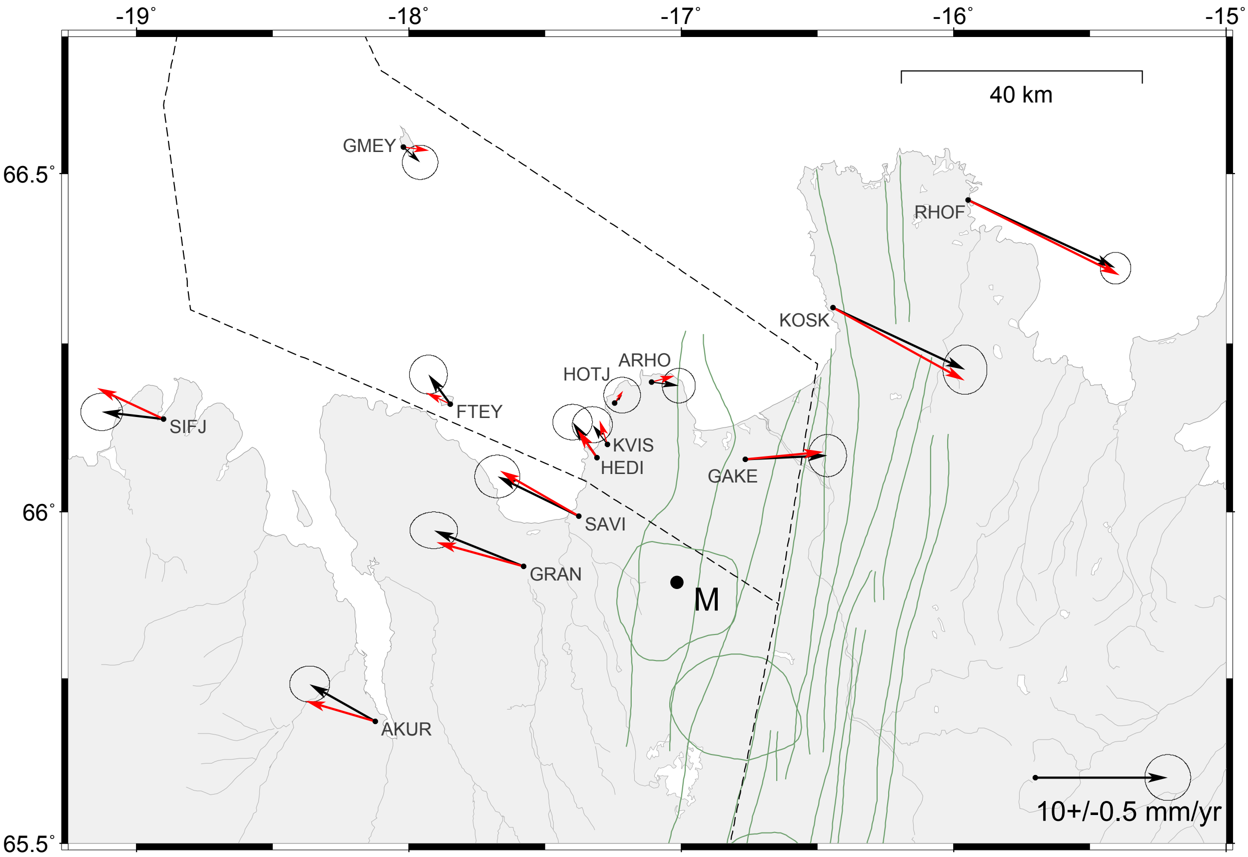

Figure 8. Horizontal GPS velocities with 95% confidence level (black) and velocity predictions of the best fit model (red). The segments of the fault model indicated with dashed lines and the location of the Mogi source **M** is marked with a black dot.

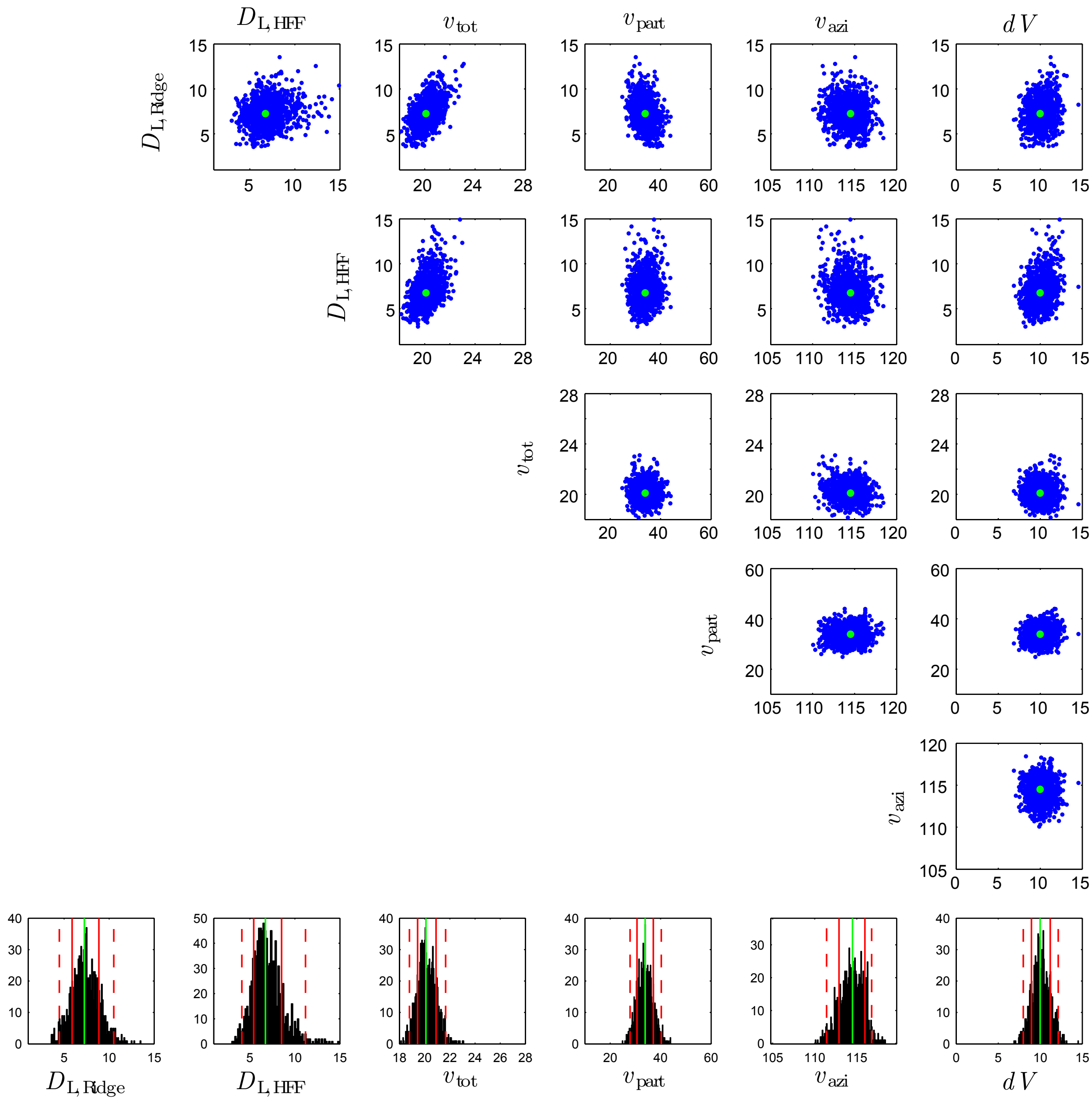

Figure 9. Parameter covariance scatter plots and histograms of the uncertainty estimation: Locking depth of the ridge segments ($D_{\mathrm{L,Ridge}}$ [km]), locking depth of the transform fault segments ($D_{\mathrm{L,HFF}}$ [km]), plate spreading motion (v_{tot} [mm/yr]), partial motion of the HFF segment (v_{part} [%]), azimuth of the total plate spreading motion (v_{azi} [N°E]) and the annual volume change of the Mogi source (dV [$\cdot 10^6$m^3/yr]). The best fit parameter is marked with green dots and lines. The 68% and 95% confidence levels are shown in red in the histograms.